Chapter 8
High Temperature Mechanical Behavior

Abstract This chapter starts with the description of the effects of elevated temperature on the deformation characteristics of materials by means of the Stress-Rupture and the Constant-Stress creep curves. The Creep Power Law for secondary creep is introduced along with the Larson and Miner creep life prediction method. Further, the deformation mechanisms in creep are described, as well as the creep fracture mechanism. Then, the ideas are applied to explain the foundations for the development of high-temperature service materials, known as refractory. The chapter ends with a brief description of the superplastic behavior that results of the combination of strengthening mechanism and high temperature behavior.

8.1 High Temperature Deformation

Some of the most important technological applications of engineering materials are at high temperature service conditions, such as: gas turbines, internal combustion engines, boilers, reactors, heat exchangers, ovens, furnaces and hot forming equipment. All these components are big and costly and their failure usually carries along high consequences (fatalities, injuries and environmental damage) and major economic losses; hence high temperature mechanical behavior is a strategic field for technological and scientific research.

The exposure of engineering materials to high temperatures has several effects, which altogether affect the mechanical behavior. The most important effects are:

1. Yield stress and tensile strength reduction.
2. Increment of ductility by increasing dislocations mobility.
3. Recovery and recrystallization of cold formed materials.
4. Grain growth.
5. Increment of diffusivity.
6. Dissolution and precipitation of second phases.
7. Incipient fusion.
8. Excessive oxidation.

J. L. González-Velázquez, *Mechanical Behavior and Fracture of Engineering Materials*, Structural Integrity 12, https://doi.org/10.1007/978-3-030-29241-6_8

All these processes are thermally activated, therefore, a sufficiently high temperature is required for them to happen, referred as *hot work*. As seen in Chap. 2, the hot work condition is relative to the material´s melting point or fusion temperature (T_f). The rule is that at working temperatures of more than $0.4T_f$, where T_f is in Kelvin degrees, the material exhibits high temperature behavior, which is primarily characterized by the strength reduction, suppression of strain hardening, and most important, the plastic strain becomes time-dependent, so the material deforms as if it was a high viscosity fluid. Such phenomenon is called *thermofluence* or most commonly *creep*.

From the engineering point of view, creep is defined as plastic deformation through time under a constant stress. After some time, creep culminates in fracture, therefore it is also a failure mechanism. It is currently known that creep is caused by thermally activated diffusive processes, and although these processes occur at any temperature, it is at high temperature ($>0.5T_f$) that it becomes of practical significance, and for that reason creep is considered a high temperature phenomenon.

Perhaps one of the most revealing manifestations about creep is the deformation and distortion of metallic structures affected by fire, as seen in the examples of Fig. 8.1, where the heat of a fire soften columns and beams, causing the plastic flow of the structural components under their own weight.

The general procedure for creep testing is described in the ASTM E139 standard and consists on applying a constant load to a smooth tensile test specimen at constant temperature and measuring the elongation as a function of time. Heating is applied by placing the test specimen inside a heating chamber, usually with a controlled atmosphere to prevent excessive oxidation. The test time may last several hours up to years, so creep tests require specialized laboratory equipment and are very costly.

Fig. 8.1 Example of creep in metallic structures affected by fire. Notice that most of the structural components deformed and collapsed under their own weight

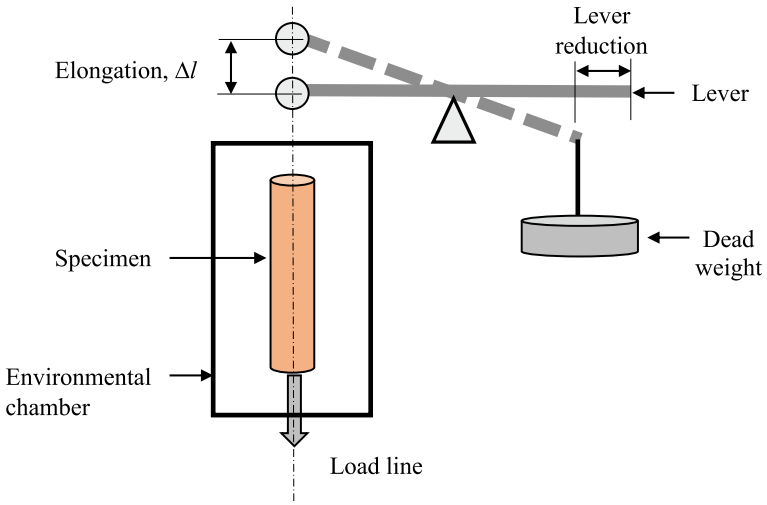

Fig. 8.2 Constant leverage creep test apparatus

In practical engineering creep tests, the load is applied by leverage system with dead weights, designed in such a way that, as the test specimen elongates, the leverage arm shortens, thus reducing the load and compensating the stress increment caused by the reduction of the specimen's cross-sectional, maintaining a fairly constant-stress. The scheme of Fig. 8.2 shows the experimental arrangement of this test.

When the constant-load creep tests for the same material are carried out at different load levels and the rupture time for each load case is recorded and plotted on logarithmic scale, then a *stress-rupture* curve is obtained, which has the shape shown in Fig. 8.3. The main characteristic of the stress-rupture test is that, as both stress and temperature increase, the rupture-time drops in an exponential way. Stress-rupture tests are conducted for periods up to 10,000 h and they are specifically applied to determine the high-temperature strength, and the minimum creep rate of engineering materials. These characteristic make the stress-rupture test useful for design, material selection and quality control purposes.

If the specimen's elongation is recorded and plotted as a function of time, a *creep curve* is obtained, which has the idealized shape shown in Fig. 8.4. The creep curve starts at an instantaneous elongation of the specimen ε_o, followed by a reduction of the *creep rate* ($d\varepsilon/dt$), then the creep rate becomes constant for most of the elapsed time and finally the creep rate increases rapidly until rupture occurs.

The constant-stress creep curve has the following characteristics:

Stage I, *transient creep*. It starts at an instantaneous initial deformation ε_o, which is proportional to the applied stress. The creep rate is initially high, but it decreases gradually until reaching a constant value. In this stage, the dislocations substructure is rearranged and some phase transformations may occur, such as dissolution or

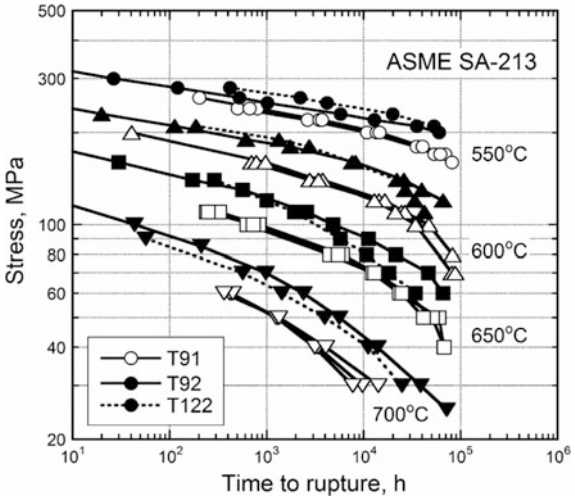

Fig. 8.3 Stress-rupture curve of a low alloy Mo-V steel. K. Image taken from: Kimura et al. [1]

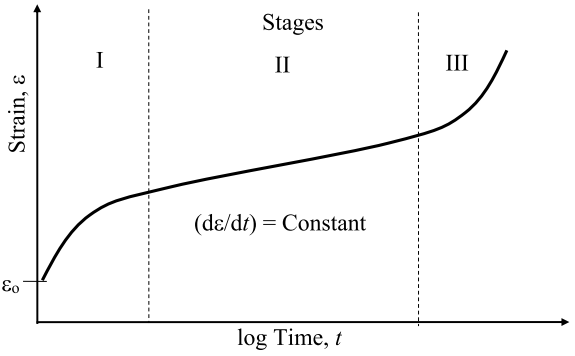

Fig. 8.4 Idealized creep curve at constant stress showing the three stages of creep

precipitation of second-phases. Once the phase transformations, the strain hardening (interaction of dislocations) and recovery processes (dislocation rearrangement and annihilation) reach a dynamic equilibrium, the creep rate becomes constant.
Stage II, *secondary creep*. In this stage, the dynamic equilibrium between the strain hardening and recovery is maintained. The creep rate in this stage is minimum and is referred to as *steady-state creep*.
Stage III, *tertiary creep*. In this stage, microstructural changes, such as precipitate coarsening and recrystallization, and the reduction in cross-section area increase the creep rate, along with an increment of vacancy diffusion and grain boundary sliding. These last two processes progress until the interconnection of grain boundary voids, lead to intergranular fractures, typical of creep failures.

Secondary creep is the most important stage, from the technological point of view, as it accounts for the longest creep period, therefore, the majority of research is aimed to estimate the creep rate in this stage.

Andrade carried out the first creep tests in 1914 and found that, most metals follow an empirical equation expressed as:

$$\varepsilon = \varepsilon_0\left(1 + \beta t^{1/3}\right)e^{kt}$$

where t stands for time, ε_o is the instantaneous initial deformation and k and β are experimental constants. It was until 1960, that Garofalo proposed an equation that fits better to the idealized creep curve and it has this form:

$$\varepsilon = \varepsilon_0 + (1 - e^{-rt}) + \left(\frac{d\varepsilon}{dt}\right)_s t$$

where $(d\varepsilon/dt)$s is the creep rate in secondary creep and r is the ratio of the transient creep rate divided by the transient creep strain.

8.2 Secondary Creep

In stage II or secondary creep, the creep rate $(d\varepsilon/dt)$, is constant and it is directly related to the applied stress (σ) by the so called *Creep Power Law*, that has the form:

$$\left(\frac{d\varepsilon}{dt}\right)_s = C\sigma^n$$

where C is an experimental constant and n is the secondary creep exponent. According to this law, the greater the stress, the greater the creep rate, as shown in Fig. 8.5. This explains why mechanical fasteners such as bolts and screws in high-temperature service get loosen sometime after they are tightened.

The steady creep rate in Stage II has been adopted as the most important design parameter for high temperature service components. The majority of codes set a creep rate limit, in which the applied stress must be adjusted based on the stress-rupture curve. For example, the typical design value for boiler and direct fire heater piping, is defined as to $(d\varepsilon/dt)s \leq 1\%/100{,}000$ h or 2.8×10^{-11} s^{-1}, so the pipe's diameter shall not expand more than 1% in 11.5 years at the design stress.

The secondary creep stage involves a process in which thermal activation provides the energy to overcome an energy barrier ΔH, moving the material thermodynamic state, from metastable, to stable. For this reason, the creep rate can be expressed by an Arrhenius type equation:

$$\left(\frac{d\varepsilon}{dt}\right)_s = Ae^{\left(\frac{-\Delta H}{RT}\right)}$$

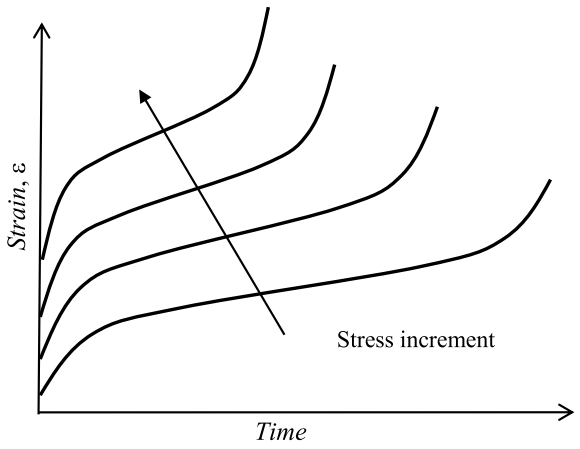

Fig. 8.5 Effect of stress on creep curves at constant temperature

where ΔH is the activation energy, T is the absolute temperature, R is the constant for ideal gases and A is a constant that depends on the material. The determination of ΔH is done by solving the previous equation with two creep rate values obtained at different temperatures in a constant-stress creep test, that is:

$$\left(\frac{d\varepsilon}{dt}\right)_1 e^{\frac{\Delta H}{RT_1}} = \left(\frac{d\varepsilon}{dt}\right)_2 e^{\frac{\Delta H}{RT_2}}$$

From which the activation energy is calculated by:

$$\Delta H = R\left[\frac{T_1 T_2}{T_1 - T_2}\right] \ln\left(\frac{\varepsilon_2}{\varepsilon_1}\right)$$

By this procedure it has been found that ΔH for secondary creep is practically equal to the activation energy for vacancy diffusion, thus, it has been concluded that secondary creep is due to vacancy flow. For the same reason, the Stage II creep mechanism is referred as to *diffusive flow*.

Table 8.1 shows values of ΔH for typical high-temperature materials. It can be observed that ΔH in materials with melting point between 1000 and 1700 °C (Cu, Fe, Ni) is three times higher than that of materials with melting point less than 600 °C (Pb, Al), whereas high melting point materials (Ta, Al_2O_3, W) have much higher ΔH and for such reason they are considered as to *refractory*.

Table 8.1 Activation energies ΔH for secondary creep of engineering materials

Metals	T_f (°C)	ΔH (kJ/mol)	Refractory materials	T_f (°C)	ΔH (kJ/mol)
Lead (Pb)	327	110	Tantalium (Ta)	2996	400
Aluminun (Al)	660	150	Alumina (Al_2O_3)	2072	620
Cooper (Cu)	1083	205	Tungsten (W)	3410	630
Ferrite (Fe α)	1535	240			
Austenite (Fe γ)	1535	280			
Nickel (Ni)	1453	300			

8.3 Creep Life Prediction

As it has been mentioned, the primary practical interest in the study of creep is to predict the rupture time. The stress-rupture test is the practical way to assess the performance of a material at high temperature, however, as mentioned before, these tests are limited by the testing time. The design life of components for high temperature service, is usually established for a minimum of 10,000 h (about 416 days), but they may be in service for 100,000 h (11.4 years) or more. The *creep design life* is defined as a minimum rupture time at the allowable stress and maximum service temperature, so if the rupture allowable stress is greater than the minimum rupture strength for the design life, either the design parameters should be modified, or the material substituted. At first, these criteria obviously requires knowledge of the stress-rupture curve, like the one shown in Fig. 8.3. But, as already mentioned, testing to obtain the rupture strength at very long periods is impractical and costly, consequently the laboratory tests to determine the creep rupture strength are be done under conditions that give rupture times within a reasonable time (generally less than 720 h, 30 days). Obviously, tests conditions that give such rupture times must be extrapolated in order to estimate the expected duration of high-temperature components. The phenomenological creep equations are a means to achieve this objective, but they require sophisticated tests to determine the necessary constants for their use.

In engineering applications, one of the most popular methods to predict creep life is the *Larson-Miller parameter curves*. This method,[1] introduced by F. R. Larson and J. Miller in 1952, is based on an Arrhenius type relation, where r is the creep rate:

$$r = A \exp(-\Delta H/RT)$$

[1]Larson and Miller [2]

where A is an experimental constant, ΔH is the creep activation energy, R is the ideal gas constant and T is the temperature. This equation can be re arranged as:

$$\Delta H/R = T(\ln A - ln\, r)$$

The rupture time is inversely proportional to r, that is:

$$t_r \propto (1/r)$$

Thus:

$$-\ln t = ln\, A - \Delta H/RT$$

Multiplying by T and converting into logarithms base 10, the following equation is obtained.

$$\Delta H/R = T(C + \log t)$$

If the ratio $\Delta H/R$ is independent from stress and temperature, then the material exhibits the same behavior at a given stress level and therefore, the term $T(C + \log t)$ is constant, and is termed as the *Larson-Miller Parameter* (*LMP*) and it allows to calculate the rupture time L in terms of *LMP*, by the equation shown below:

$$\log_{10} L = \frac{1000\, LMP(\sigma)}{T} - C$$

where L is in hours and T is in absolute degrees and $LMP(\sigma)$ is calculated at the evaluation stress level in MPa. Figure 8.6 sows the $LMP(\sigma)$ values for a ferritic steel, L in hours, T is in degrees Kelvin and σ in MPa. The equations to calculate $LMP(\sigma)$ of several materials are provided in the Annex 10B of the API 579-1/ ASME FFS-1 2016. For example, the equation for average $LMP(\sigma)$ of Low Carbon Steel:

$$LMP(\sigma, ksi) = 39.793713 - 0.15443414\sigma - 2.6260065\ \ln \sigma$$

The value of C for each material has to be experimentally determined by at least two sets of time-temperature creep tests at constant stress, by the following procedure.

Assuming that $\Delta H/R$ is a constant at a given stress level, it can be written that:

$$C = (T_2 \log t_2 - T_1 \log t_1)/(T_1 - T_2)$$

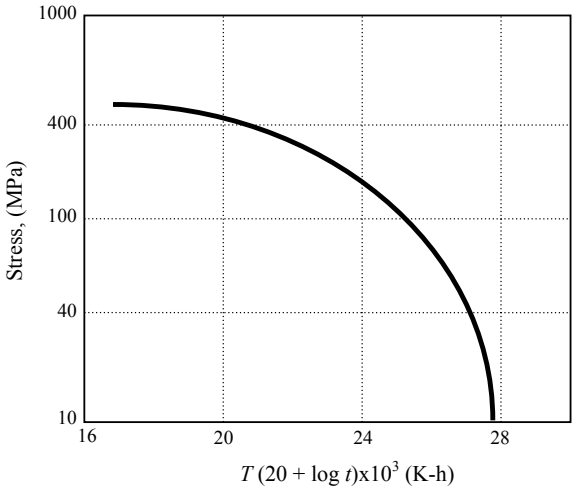

Fig. 8.6 Larson-Miller Parameter curve as a function of stress for a ferritic steel

A more precise evaluation can be obtained graphically by the equation:

$$\log t = -C + Cte/T$$

The experimental data log(t) versus. $1/T$ for different stress levels are plotted and the value of C is determined by the intersection of the extrapolation to the origin where $1/T = 0$, as shown in Fig. 8.7. The values of C for some steels commonly used in high-temperature applications are given in Table 8.2. As it can be noticed, the average value of C is 20 for most ferrous alloys, hence LMP is frequently expressed as $T(20 + \log t)$, where T is in degrees Kelvin and t in hours.

The following example illustrates the use of the Larson-Miller Parameter.

Example Determine the rupture time for an S-590 steel at a stress σ = 100 MPa at 1000 °C. Repeat the calculation for: T =700 °C and T =1000 °C, σ = 50 MPa.

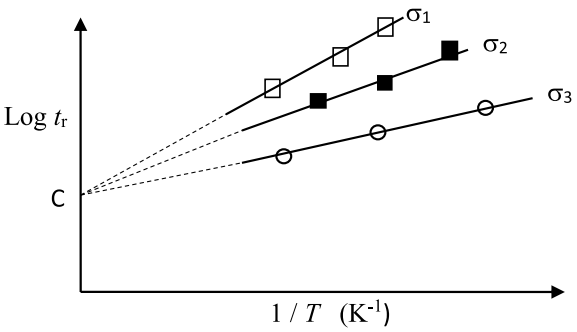

Fig. 8.7 Determination of the Larson-Miller Parameter from the experimental data log tr versus $1/T$ obtained at different stress levels and extrapolated at $1/T = 0$

Table 8.2 Constant C for steels (T in degrees Kelvin and t in hours)

Alloy	C (h)
Low carbon steel	18
Stainless steel 18-8	18
Stainless steel 18-8-Mo	17
Steel 2 ¼ Cr-1 Mo	23
Steel S 590	20
Steel Cr-Mo-Ti-B	22

Solution

From Fig. 8.6 at σ = 100 MPa, T (20 + log t)=25,200
$\log t = (25{,}200/T) - 20 = 25{,}200/1273 - 20 = -0.2$
That is, t = 0.62 h (37.5 min)
For $T = 500\,^{\circ}\mathrm{C}$, $\log t = 25,200/973 - 20 = 5.9$
That is, t = 7.93 × 105 h (90.5 years)
For the stress of 50 MPa, T(20 + log t) =27,200
Clearing : $\log t = (27{,}200/T) - 20 = 27,200/1273 - 20 = 1.37$
That is, t = 23.3 h.

From the previous example it is clear that temperature has a much greater effect than stress on the creep rupture time. The practical consequence of this is that it is more convenient to prevent overheating than to reduce operation stress to increase the creep rupture time. This may be counterproductive for internal combustion engine and process equipment, as in most of these applications, the higher the temperature, the higher efficiency, hence many efforts in creep research are aimed to the development of materials able to operate at higher temperatures in combination with high strength.

8.4 Deformation Mechanisms in Creep

Deformation mechanisms in creep primarily depend on slip and grain boundary sliding. At relatively low temperatures (<0.3T_f) dislocation slip mechanisms prevail, but at high temperatures (>0.5T_f), mechanisms based on diffusion and grain boundary glide become predominant, however, the general condition is that these mechanisms may simultaneously occur. The principal creep deformation mechanisms are:

Dislocation climb. When dislocations move through a crystal at high-temperature under high stresses, thermal activation helps to overcome the lattice friction and short-range obstacles located on the slip planes. However, at intermediate and low stress levels, the dislocation glide is assisted by vacancy diffusion by a process called as *dislocation climb*. Dislocation climb is an out-of-plane movement, which occurs by vacancy diffusion, as schematically

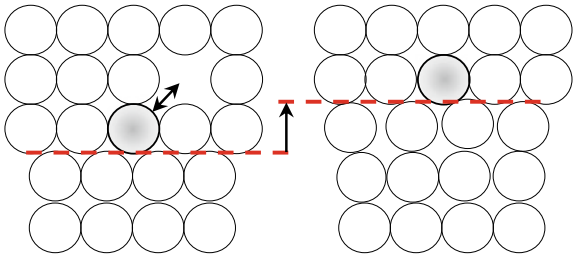

Fig. 8.8 Climb of an edge dislocation by vacancy exchange

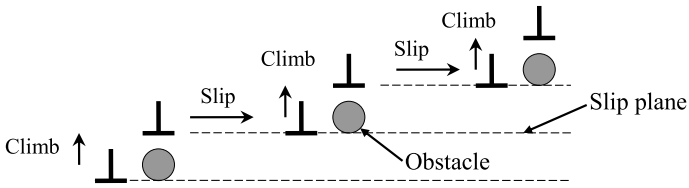

Fig. 8.9 Dislocation climb to overcome non-shearing obstacles

shown in Fig. 8.8. When a vacancy exchanges its place with the atom located on the dislocation line (shaded circle in Fig. 8.8), the segment "climbs" one atomic position in the lattice. If another vacancy moves towards the dislocation line, the process is repeated, until the entire dislocation line climbs. This movement produces shear strain of the crystal, and just like stress-activated glide.

Dislocation climb also assist dislocations overcomes long-range obstacles such as precipitate particles. Once the dislocation overcame the obstacle by climb, it continues gliding until it faces another obstacle, and then the climb process repeats, as schematically in Fig. 8.9.

In 1960, Weertman proposed a model to estimate the strain rate in secondary creep by dislocation movement, which is applicable at temperatures higher than $0.5T_f$, known as the *power-law creep*, represented by the following equation:

$$\left(\frac{d\varepsilon}{dt}\right)_s = \left[\frac{AD_{eff}Gb}{kT}\right]\left(\frac{\sigma}{G}\right)^n$$

where D_{eff} and A *and* n are experimental constants.

Creep by diffusive flow. This mechanism was proposed by Nabarro-Herring in 1950, and it involves the grains deformation by massive vacancy flow. The deformation flow is from zones under compression stresses, towards tension stressed zones. Simultaneously, atoms and vacancies flow in the opposite direction, producing elongation, as schematically shown in Fig. 8.10.

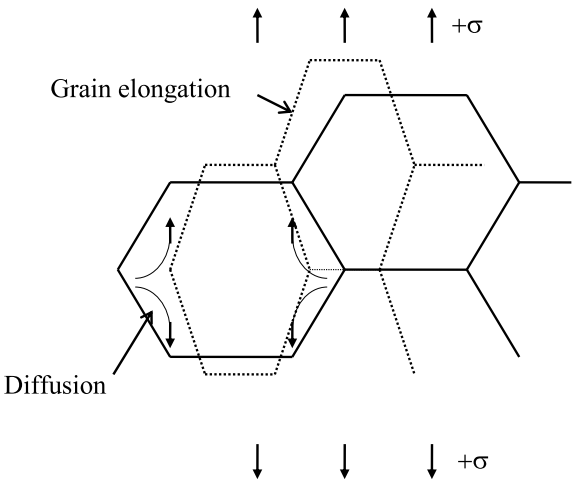

Fig. 8.10 Nabarro-Herring model of creep by diffusive flow

The phenomenological equation for the diffusive-flow mechanism is:

$$\left(\frac{d\varepsilon}{dt}\right)_s = \frac{14\sigma b^3 D_v}{kTd^2}$$

where d is the grain size and Dv is the lattice diffusion coefficient. At lower temperatures, close to the limit of the hot work regime, the diffusive-flow mechanism is substituted by a grain boundary sliding mechanism, for which Coble, in 1963, proposed the following model:

$$\left(\frac{d\varepsilon}{dt}\right)_s = \frac{60\sigma b^4 D_{gb}}{kTd^3}$$

The previous equations show that the grain size plays an important role in deformation in creep, since it appears raised at the cube power. This indicates that coarse grain materials have higher creep strength. Such findings have led to the development of coarse grain materials, and even single-crystals in order to improve their performance at high temperatures, as it will be discussed further in this chapter.

8.5 Creep Fracture

Generally, creep fractures are intergranular, since at high temperatures, above the equicohesive temperature (T_{eq}), as described in Sect. 4.3, the grain boundaries are weaker than the grains. The intergranular fracture mechanism in creep results from the combination of grain boundary cavitation and sliding. At macroscopic scale,

Fig. 8.11 Macroscopic (left) and microscopic (right) appearance of a typical creep fracture

creep fractures feature small plastic deformation, minimum neck formation and high surface roughness, whereas at microscopic scale the fracture path is intergranular and the grain facets are covered with numerous dimples. Figure 8.11 shows an example of a typical creep fracture.

At temperatures far above T_{eq} and low stress levels, creep deformation is dominated by grain boundary sliding, which favors intergranular fracture. Intergranular fracture in creep occurs by to two basic mechanisms:

1. Grain boundary slip
2. Grain boundary cavitation.

Grain boundary sliding causes decohesion of grain boundary triple joints, forming wedge-shaped cavities, termed as *w-type*, as schematically shown in Fig. 8.12. The *w-type* cavities are formed preferentially in grain boundaries aligned to the maximum shear stress, thus in components under uniaxial tensile loads, they will be at around 45 degrees form the load line.

The condensation of vacancies in the grain boundaries, on the other hand, originates the formation of round cavities termed as r-*type*. When the number and size of the *r-type* cavities is high enough, they coalesce causing an intergranular fracture with little plastic strain associated to it.

The growth rate of *r-type* cavities is controlled by vacancy diffusion and power-law creep, according to the following equation.

$$dr/dt = C\,D_V r^m \sigma^n$$

where *dr/dt* is the cavity growth rate, *Dv* is the vacancy diffusivity coefficient, *r* is the cavity size, *m* is an experimental constant, and *n* is the power-law creep exponent. An interesting aspect of *r-type* grain boundary cavitation is that, according to the previous equation, *dr/dt* depends on the cavity size, meaning that large cavities grow faster than smaller ones. Additionally, for an *r-type* cavity to grow, the work supplied by stress has to be greater than the void surface energy γ_s. If this condition is not met, small cavities will reduce their size until collapse.

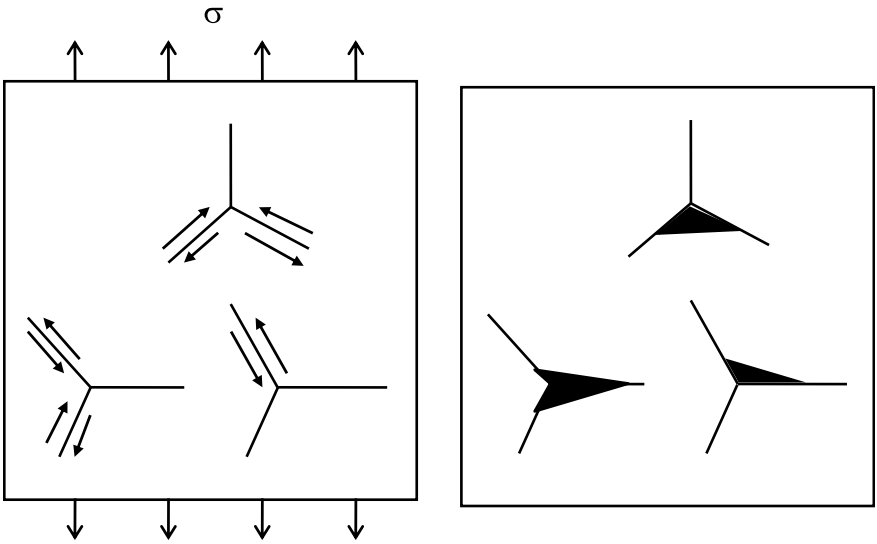

Fig. 8.12 Formation of *w-type* cavities by grain boundary sliding

The cavity minimum size (r_o) in order to maintain a stable growth condition can be calculated by:

$$r_o = 2\gamma_s/\sigma_{GB}$$

where σ_{GB} is the tension stress on the grain boundary. This equation indicates that r-*type* cavitation is favored by high tension stresses and low γ_s values. Since γ_s increases in proportion to the content of solid-solution forming elements, solid solution alloys have better creep strength, because r-*type* voids have to reach larger sizes in order to grow and coalesce, so the intergranular fracture process is delayed.

Another important factor is that *r-type* cavitation preferably occurs in grain boundaries oriented in direction nearly perpendicular to the maximum tension stress, as shown in Fig. 8.13.

Creep crack growth. Creep fracture can also occur locally, at specific locations such as pre-existing cracks or stress concentrators, because, they form local highly stressed plastic zones, so the creep rate increases, and the creep rupture time is drastically reduced. The creep crack growth mechanism is schematically depicted in Fig. 8.14. This is controlled by the cavity growth rate, which in turn, depends on the stress magnitude at the crack tip. According to fracture mechanics, the extension of crack in a strained body is determined by the energy release rate, which results from the balance between the work done by the tractions and the stored strain energy, as described by Rice's *J-integral* (see Sect. 6.4 in this book). But, since creep is a time-dependent process *J* has to be expressed as a function of time, *dJ/dt*. This derivate is typically represented by the symbol *C**, representing the time-dependent crack energy release rate. It has been experimentally found that:

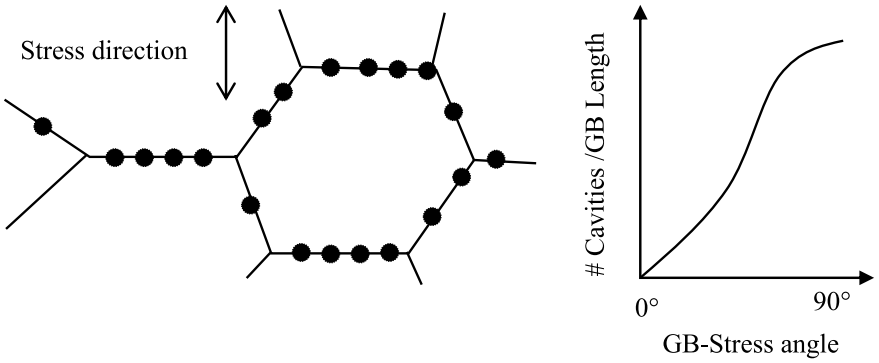

Fig. 8.13 Distribution of cavities in terms of grain boundary orientation with respect to tension stress

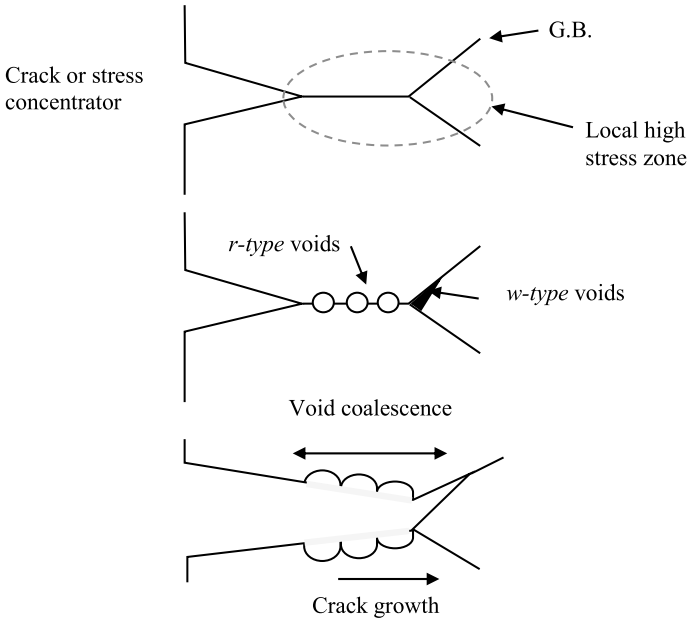

Fig. 8.14 Local creep crack growth mechanism by cavitation of grain boundaries at stress concentrators

$$\frac{da}{dt} = A(C^*)^n$$

where (da/dt) is the crack growth rate, A and n are experimental constants.

8.6 High Temperature Materials

The phenomenological equations along with the deformation mechanisms of creep are useful to predict the effect of variables such as stress, temperature, microstructure and so forth. Research on creep and creep-strength have set the foundations for the development of alloys and materials for high-temperature service, known as *refractory materials*. At first, refractory materials must have a high melting point and high Homologous Temperature, because these two are determining factors on whether deformation is within the creep regime or not. Second, refractory materials should have resistance to oxidation and high temperature corrosion, otherwise their usefulness is limited, such as the case of tungsten, which has high creep strength, but its oxidation strength is so low that when exposed to air at high temperature it oxides completely in a matter of few minutes.

In general, the phenomenological equation that describes creep can be generalized as to:

$$\left(\frac{d\varepsilon}{dt}\right)_s = Cte\frac{\sigma D}{TGd^n}$$

where $(d\varepsilon/dt)_s$ is the secondary creep rate, D is the diffusivity coefficient, G is the shear elastic modulus, d is the grain size and Cte is a constant depending on the material. According to this expression, materials with *fcc* structure are more resistant to heat than materials with less-compact structures as they have lower D values. Likewise, materials with high G will have a better performance at high temperatures. Tungsten, alumina, tantalum, as well as, austenitic stainless steels, nickel and cobalt based alloys exhibit these characteristics and therefore they are the main group of materials for high temperature applications.

A term of great importance in the above equation is the grain size (d) because the exponent n varies between 2 and 3, thus moderate grain size increments, significantly increase creep strength. In addition, as mentioned in the previous sections, the grain boundary cavity distribution depends on the orientation with respect to the direction of the applied stress, thus the grains perpendicular to the stress direction have the maximum cavitation, whereas the grain boundaries parallel to the stress, practically do not suffer it. This has led to the design of coarse-columnar grain materials, where the long direction of the grains is oriented parallel to the maximum principal stress direction in order to increase creep strength. Such strategy has gone as far as developing materials without grain boundaries at all, that means,

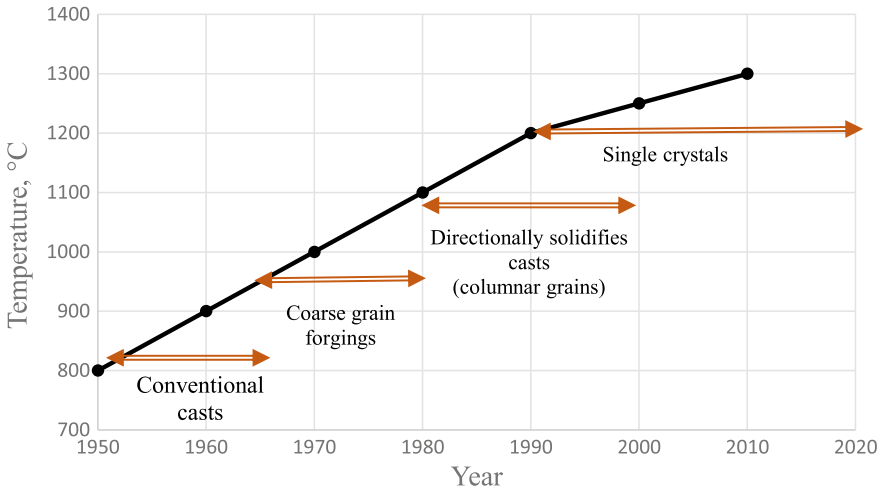

Fig. 8.15 Evolution of creep strength and grain size of materials for blades used in the combustion section of gas turbines and airplane engines

single-crystals. Figure 8.18 shows the evolution of materials for the manufacture of airplane turbine blades in terms of the grain size structure (Fig. 8.15).

The next microstructural characteristic that improves creep strength is size and distribution of second-phase precipitates. At first, the precipitates should be stable and coarse enough to reduce grain boundary sliding; second, they should have a high melting point, and third, they should have interstitial alloying elements. This combination reduces diffusivity, dislocation climb and diffusive flow altogether. These characteristics are featured by nickel-base super alloys, constituted by cuboidal-shaped gamma precipitates, with ordered crystalline structure, which are formulated and specially heat treated to obtain a microstructure like the one shown in Fig. 8.16. Other developments are metallic alloys hardened by alumina or silicon carbide particles, in order to maximize the stability second phase particles. These materials are manufactured by powder metallurgy techniques and exhibit high-temperature strengths as much as 20 times higher than that those of conventional alloys. Table 8.3 lists some of the typical materials for high temperature applications, with their main characteristics and maximum service temperature.

8.7 Superplastic Behavior

Superplastic behavior, also termed *superplasticity* is the ability of some materials to show great elongations in tension, as much as several thousand per cent, so their appearance after a tension test is like the schematic representation of Fig. 8.17. Not long ago, superplasticity was considered as laboratory-curiosity, but currently the need for making complex pieces and reduce manufacturing costs has made

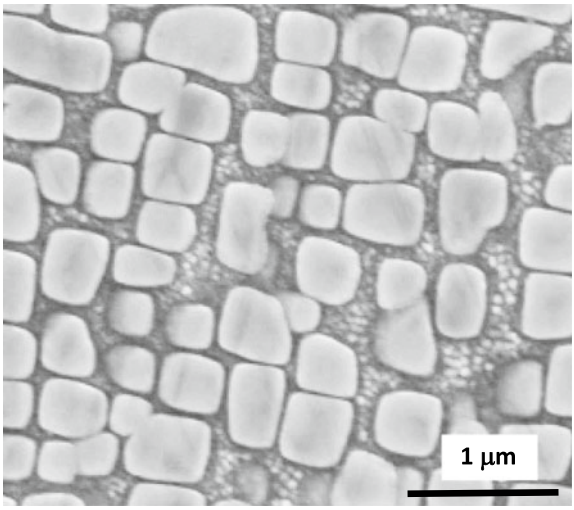

Fig. 8.16 Microstructure of a nickel-base super alloy for high temperature use

Table 8.3 Typical materials for high temperature applications

Material	Types	Max. service temp. (°C)
High alloy solid solution steels	Austenitic, series 304, 316 y 321 Forged o centrifugal cast	600
Low alloy ferritic steels strengthened by carbides	Up to 4% Cr + (Mo, V) Forged or rolled	650
Nickel Base Superalloys: Ni + (Cr, W, Co)	Supersaturated matrix with ordered precipitates. Directional solidification with columnar grain or single crystal	950
Oxides and refractory carbides: Al_2O_3, SiC, Si_3N_4	Monolithic, thermal spray or dispersion strengthened mechanically alloyed	1300

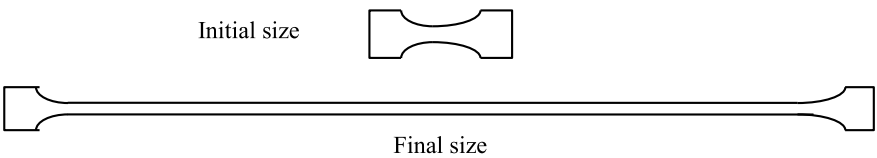

Fig. 8.17 Schematic illustration of a tension specimen after superplastic deformation

superplasticity commercially attractive. To achieve superplastic behavior, it is required that the material does not develop necks during tensile strain, so the mechanism of ductile fracture by nucleation and coalescence of internal voids has to be suppressed (see Chap. 6), therefore the material may continue elongating without rupture. Such condition is obtained if the material has a high strain hardening coefficient, as it will be shown next.

From Garofalo's equation, the equation for secondary creep deformation can be expressed as:

$$\sigma = Ct\left(\frac{d\varepsilon}{dt}\right)^{m'}$$

where σ is the real stress, ε is the real strain, t is time, m' is the dynamic strain hardening coefficient ad Ct is an experimental constant. Stress is given by $\sigma = F/A$, where F is the load and A is the cross section area. If the deformation is uniform, $d\varepsilon/dt = dA/dt$, then it can be shown that:

$$-\frac{dA}{dt} = \left(\frac{F}{Ct}\right)^{\frac{1}{m'}}\left(\frac{1}{A^{1-m'}}\right)$$

According to this equation, as m' increases, the dA/dt diminishes, and if m' approaches to 1.0 (linear strain hardening), dA/dt becomes close to zero, which means that necks will not be formed and thus the material will be superplastic. Superplastic behavior has been observed in many alloy systems and it is fundamentally a dynamic strain-induced precipitation phenomenon. Researchers have found that superplastic materials must have m' values higher than 0.5, in addition to complying with the following requirements:

(1) Low strain rates, from 10^{-4} to 10^{-6} s^{-1}
(2) Temperature above $0.5T_f$
(3) Grain size less than 10 microns
(4) Dynamic second phase precipitation.

There is still controversy about the superplastic deformation mechanism, but it is generally acknowledged that it involves extensive grain boundary sliding, where the deformation of equiaxial is accommodated by grain rotation. During superplastic deformation, the crystalline texture is destroyed, and therefore no cell dislocations nor subgrains are formed, which indicates that the dislocations are quickly annihilated as they appear, thus making strain hardening a dynamic process too.

To determine whether a material can be superplastic, a Stress vs. Strain-rate plot must be constructed from tension tests at several strain rates. The stress-strain rate relation can be rewritten logarithmically as:

$$\log, \sigma = \log Ct + m' \log(d\varepsilon/dt)$$

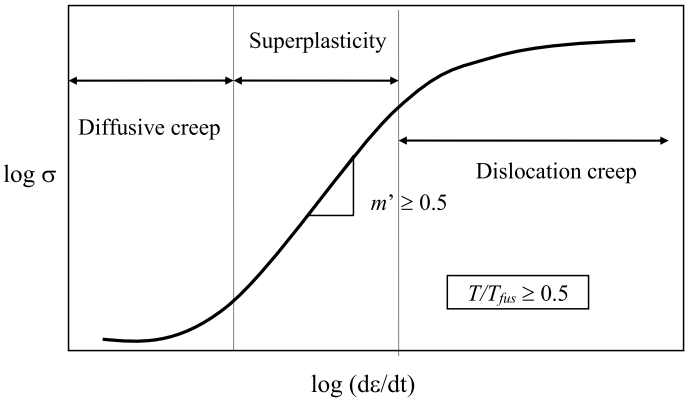

Fig. 8.18 Stress-Strain rate curve to determine the potential for superplastic behavior

Thus, by plotting the experimental data of strain rate and stress in a log-log scale, as shown in Fig. 8.18, the slope of the straight portion of the plot is the coefficient m', then if $m' > 0.5$ the material may be superplastic. This condition is achieved at intermediate strain rates, since at low and high strain rates, the deformation mechanisms are diffusive creep and dislocation creep, respectively, therefore, the material will not exhibit large elongations, because the aforementioned dynamic processes do not occur.

References

1. Kimura K, Sawada K, Kushima H (2012) Creep ductility of creep strength enhanced ferritic steels. J Pressure Vessel Technol 134
2. Larson FR, Miller J (1952) Transactions ASME 74:765–771